ISSN 1674-1056
http://cpb.iphy.ac.cn
http://iopscience.iop.org/cpb
中国物理 B
Chinese Physics
中国物理
Chinese Physics B

Internal and near-surface fields for a chiral sphere under arbitrary laser beam illumination

Bi-Da Su(苏必达), Ming-Jun Wang(王明军), Yue Peng(彭月), Su-Hui Yang(杨苏辉), Hua-Yong Zhang(张华永)

Citation: Chin. Phys. B . 2019, 28(6): 064210. **doi:** 10.1088/1674-1056/28/6/064210
Journal homepage: http://cpb.iphy.ac.cn; http://iopscience.iop.org/cpb

What follows is a list of articles you may be interested in

Electromagnetic scattering of charged particles in a strong wind-blown sand electric field

Xingcai Li(李兴财), Xuan Gao(高璇), Juan Wang(王娟)

Chin. Phys. B . 2019, 28(3): 034208. **doi:** 10.1088/1674-1056/28/3/034208

Experimental determination of distributions of soot particle diameter and number density by emission and scattering techniques

Huawei Liu(柳华蔚), Shu Zheng(郑树)

Chin. Phys. B . 2019, 28(1): 014206. **doi:** 10.1088/1674-1056/28/1/014206

Polarization-based range-gated imaging in birefringent medium:Effect of size parameter

Heng Tian(田恒), Jing-Ping Zhu(朱京平), Shu-Wen Tan(谭树文), Jing-Jing Tian(田晶晶), Yun-Yao Zhang(张云尧), Xun Hou(侯洵)

Chin. Phys. B . 2018, 27(12): 124203. **doi:** 10.1088/1674-1056/27/12/124203

Scanning the energy dissipation process of energetic materials based on excited state relaxation and vibration-vibration coupling

Wen-Yan Wang(王文岩), Ning Sui(隋宁), Li-Quan Zhang(张里荃), Ying-Hui Wang(王英惠), Lin Wang(王琳), Quan Wang(王权), Jiao Wang(王娇), Zhi-Hui Kang(康智慧), Yan-Qiang Yang(杨延强), Qiang Zhou(周强), Han-Zhuang Zhang(张汉壮)

Chin. Phys. B . 2018, 27(10): 104205. **doi:** 10.1088/1674-1056/27/10/104205

Rapid measurement of transmission matrix with the sequential semi-definite programming method

Zhenfeng Zhang(张振峰), Bin Zhang(张彬), Qi Feng(冯祺), Huimei He(何惠梅), Yingchun Ding(丁迎春)

Chin. Phys. B . 2018, 27(8): 084201. **doi:** 10.1088/1674-1056/27/8/084201

Internal and near-surface fields for a chiral sphere under arbitrary laser beam illumination*

Bi-Da Su(苏必达)[1,2], Ming-Jun Wang(王明军)[3,†], Yue Peng(彭月)[2], Su-Hui Yang(杨苏辉)[1], and Hua-Yong Zhang(张华永)[4]

[1] *Department of Photoelectric Engineering, Beijing Institute of Technology, Beijing* 100854, *China*
[2] *Science and Technology on Optical Radiation Laboratory, Beijing* 100854, *China*
[3] *School of Automation and Information Engineering, Xi'an University of Technology, Xi'an* 710048, *China*
[4] *School of Electronics and Information Engineering, Anhui University, Hefei* 230039, *China*

(Received 20 February 2019; revised manuscript received 1 April 2019; published online 29 May 2019)

A general scheme for the investigation of scattering by a chiral sphere under arbitrary monochromatic laser beam illumination is presented. The scattered and internal fields are expanded by using appropriate spherical vector wave functions, and their expansion coefficients are determined by the boundary conditions and the projection method. Targeting multiple incidence forms such as Gaussian beam, Hermite–Gaussian beam, doughnut mode beam and zero-order Bessel beam, the influence and propagation of near-surface intensity field for a chiral sphere are analyzed. These properties are very important for studying the properties of chiral media, and for manipulating the optical tweezers and super-resolution imaging of particles.

Keywords: scattering, chiral sphere, monochromatic laser beamirradiation, field intensity distribution

PACS: 42.25.Fx, 78.20.Ek, 42.55.–f, 42.60.Jf **DOI:** 10.1088/1674-1056/28/6/064210

1. Introduction

After decades of development, laser technology has spread widely into a variety of applications like atmospheric detection, biotechnology, chemical technology, laser optical tweezers and laser radar detection. In order to precisely describe and manipulate lasers, the demand for an in depth understanding of the interaction between laser beam and material has become increasingly urgent. The chiral particle, especially the chiral sphere, has become one of the widely used theoretical models due to its ability to accurately describe light-particle interactions. Many macromolecules and biological structures in nature, including haze and aerosol, are, in general, composed of chiral media, which leads to multiple intriguing effects when interacting with light. Light scattering of symmetric chiral sphere under different forms of light beams is important for laser radar transmission mode selection, target recognition, microwave technology, atmospheric science, laser tweezers and laser field acquisition efficiency research. Using vector wave functions, Bohren analyzed the scattering of plane waves by spheres with inherent optical activity.[1] Since then, structured laser beams have been utilized to investigate various fields with practical significance, like optical capture and manipulation,[2] atomic optics,[3] and imaging.[4] The scattering of Hermite–Gaussian beams from the chiral sphere has been studied by calculating the multipole field under the incidence of conventional Hermite-Gaussian beams.[5] The analytical solutions for the scattering of chiral spheres irradiated by Gaussian and Laguerre–Gaussian beams have been documented.[6–8] In all these papers, the incident electromagnetic (EM) fields were expanded into an infinite series of partial or spherical vector wave functions (SVWFs), which are, however, usually difficult to obtain, especially for a large number of structured laser beams. In this paper, a general expression of EM field scattered by a chiral sphere being irradiated by an arbitrary monochromatic laser beam is given, for which the incident EM field only needs to be explicitly described.

The rest of this paper is organized as follows. In Section 2, a theoretical calculation method for the scattered field of chiral spheres irradiated by monochromatic laser is proposed. In Section 3, numerical results of the normalized internal and near-surface field intensity distribution (FID) are given for Gaussian, Hermite-Gaussian, doughnut mode and zero-order Bessel beams (ZOBB). The effects of different light fields on propagation are analyzed. Finally, we draw some conclusions in Section 4.

2. Formulation

As a schematic diagram, figure 1 shows a chiral sphere irradiated by a monochromatic laser beam, which propagates in free space and along the positive z' axis in the Cartesian coordinate system $O'x'y'z'$ (laser beam coordinate system). A chiral sphere is attached to the system $Oxyz$ (parallel to $O'x'y'z'$),

*Project supported by the National Natural Science Foundation of China (Grant No. 61771385) and the Industrial Research of Science and Technology Plan of Shaanxi Province, China (Grant No. 2016GY-082).

†Corresponding author. E-mail: wmjxd@aliyun.com

© 2019 Chinese Physical Society and IOP Publishing Ltd

with origin O located at (x_0', y_0', z_0') in $O'x'y'z'$. In this paper, the time-dependent part of the EM field is assumed to be $\exp(-\mathrm{i}\omega t)$.

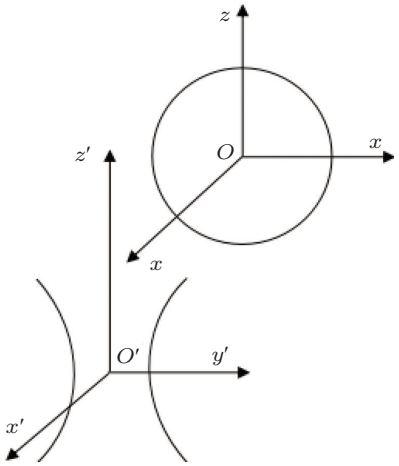


Fig. 1. Chiral sphere illuminated by monochromatic laser beam.

The scattered fields by the chiral sphere can be expanded by using the SVWFs of the third kind with respect to the system $Oxyz$ in the following form:

$$\boldsymbol{E}^{\mathrm{s}} = E_0 \sum_{n=1}^{\infty} \sum_{m=-n}^{n} [a_{mn} \boldsymbol{M}_{mn}^{r(3)}(k_0 \boldsymbol{r}) + b_{mn} \boldsymbol{N}_{mn}^{r(3)}(k_0 \boldsymbol{r})], \tag{1}$$

$$\boldsymbol{H}^{\mathrm{s}} = -\mathrm{i} \frac{E_0}{\eta_0} \sum_{n=1}^{\infty} \sum_{m=-n}^{n} [a_{mn} \boldsymbol{N}_{mn}^{r(3)}(k_0 \boldsymbol{r}) + b_{mn} \boldsymbol{M}_{mn}^{r(3)}(k_0 \boldsymbol{r})], \tag{2}$$

where $k_0 = \omega\sqrt{\mu_0 \varepsilon_0}$ and $\eta_0 = \sqrt{\mu_0/\varepsilon_0}$ are the free space wave number and characteristic impedance, respectively, and a_{mn} and b_{mn} are the expansion coefficients.

The constitutive relations of a chiral medium can be described by[6,7]

$$\boldsymbol{D} = \varepsilon_0 \varepsilon_{\mathrm{r}} \boldsymbol{E} + \mathrm{i}\kappa\sqrt{\mu_0/\varepsilon_0}\boldsymbol{H}, \tag{3}$$

$$\boldsymbol{B} = \varepsilon_0 \varepsilon_{\mathrm{r}} \boldsymbol{H} + \mathrm{i}\kappa\sqrt{\mu_0/\varepsilon_0}\boldsymbol{E}, \tag{4}$$

where κ, μ_{r}, and ε_{r} are the chirality parameter, relative permeability, and permittivity of chiral medium, respectively.

As discussed in Refs. [6]–[8], the SVWFs of the first kind can be used to expand the fields within the chiral sphere (internal fields) as follows:

$$\boldsymbol{E}^{\mathrm{w}} = E_0 \sum_{n=1}^{\infty} \sum_{m=-n}^{n} \{c_{mn}[\boldsymbol{M}_{mn}^{r(1)}(k_+ \boldsymbol{r}) + \boldsymbol{N}_{mn}^{r(1)}(k_+ \boldsymbol{r})] + d_{mn}[\boldsymbol{M}_{mn}^{r(1)}(k_- \boldsymbol{r}) - \boldsymbol{N}_{mn}^{r(1)}(k_- \boldsymbol{r})]\}, \tag{5}$$

$$\boldsymbol{H}^{\mathrm{w}} = -\mathrm{i} \frac{E_0}{\eta} \sum_{n=1}^{\infty} \sum_{m=-n}^{n} \{c_{mn}[\boldsymbol{M}_{mn}^{r(1)}(k_+ \boldsymbol{r}) + \boldsymbol{N}_{mn}^{r(1)}(k_+ \boldsymbol{r})] - d_{mn}[\boldsymbol{M}_{mn}^{r(1)}(k_- \boldsymbol{r}) - \boldsymbol{N}_{mn}^{r(1)}(k_- \boldsymbol{r})]\}, \tag{6}$$

where $\eta = \eta_0\sqrt{\mu_{\mathrm{r}}/\varepsilon_{\mathrm{r}}}$ and $k_\pm = k_0(\sqrt{\mu_{\mathrm{r}}\varepsilon_{\mathrm{r}}} \pm \kappa)$.

The SVWFs of the first or third kind in Eqs. (1), (2), and Eqs. (5) and (6) indicate that the radial dependence functions in them are respectively the spherical Bessel or Hankel functions of the first kind.[9]

The boundary conditions over the sphere surface can be represented by

$$\begin{cases} \hat{r} \times (\boldsymbol{E}^{\mathrm{s}} + \boldsymbol{E}^{\mathrm{i}}) = \hat{r} \times \boldsymbol{E}^{\mathrm{w}}, & \text{at } r = r_0, \\ \hat{r} \times (\boldsymbol{H}^{\mathrm{s}} + \boldsymbol{H}^{\mathrm{i}}) = \hat{r} \times \boldsymbol{H}^{\mathrm{w}}, & \text{at } r = r_0, \end{cases} \tag{7}$$

where $\boldsymbol{E}^{\mathrm{i}}$ and $\boldsymbol{H}^{\mathrm{i}}$ are the incident electric and magnetic field, and r_0 is the sphere radius.

Substituting Eqs. (1), (2), (5), (6) into Eq. (7), we have

$$\begin{aligned} &\hat{r} \times E_0 \sum_{n=1}^{\infty} \sum_{m=-n}^{n} [a_{mn} \boldsymbol{M}_{mn}^{r(3)}(k_0 r_0) + b_{mn} \boldsymbol{N}_{mn}^{r(3)}(k_0 r_0)] + \hat{r} \times \boldsymbol{E}^{\mathrm{i}} \big|_{r=r_0} \\ &\quad = \hat{r} \times E_0 \sum_{n=1}^{\infty} \sum_{m=-n}^{n} \{c_{mn}[\boldsymbol{M}_{mn}^{r(1)}(k_+ r_0) + \boldsymbol{N}_{mn}^{r(1)}(k_+ r_0)] + d_{mn}[\boldsymbol{M}_{mn}^{r(1)}(k_- r_0) - \boldsymbol{N}_{mn}^{r(1)}(k_- r_0)]\}, \end{aligned} \tag{8}$$

$$\begin{aligned} &\hat{r} \times E_0 \sum_{n=1}^{\infty} \sum_{m=-n}^{n} [a_{mn} \boldsymbol{N}_{mn}^{r(3)}(k_0 r_0) + b_{mn} \boldsymbol{M}_{mn}^{r(3)}(k_0 r_0)] + \mathrm{i}\eta_0 \hat{r} \times \boldsymbol{H}^{\mathrm{i}} \big|_{r=r_0} \\ &\quad = \hat{r} \times E_0 \frac{\eta_0}{\eta} \sum_{n=1}^{\infty} \sum_{m=-n}^{n} \{c_{mn}[\boldsymbol{M}_{mn}^{r(1)}(k_+ r_0) + \boldsymbol{N}_{mn}^{r(1)}(k_+ r_0)] - d_{mn}[\boldsymbol{M}_{mn}^{r(1)}(k_- r_0) - \boldsymbol{N}_{mn}^{r(1)}(k_- r_0)]\}. \end{aligned} \tag{9}$$

By substituting spherical harmonic functions $\mathrm{Y}_{mn}(\theta, \phi) = \mathrm{P}_n^m(\cos\theta)\mathrm{e}^{\mathrm{i}m\phi}$ into the vector spherical harmonics (VSHs) denoted as $\boldsymbol{m}_{mn}(\theta, \phi)$ and $\boldsymbol{n}_{mn}(\theta, \phi)$, the latter can be written as

$$\boldsymbol{m}_{mn}(\theta, \phi) = \nabla \times [\boldsymbol{r}\mathrm{Y}_{mn}(\theta, \phi)] = \left[\mathrm{i}m \frac{\mathrm{P}_n^m(\cos\theta)}{\sin\theta}\hat{\theta} - \frac{\mathrm{d}\,\mathrm{P}_n^m(\cos\theta)}{\mathrm{d}\theta}\hat{\phi}\right] \mathrm{e}^{\mathrm{i}m\phi}, \tag{10}$$

$$\boldsymbol{n}_{mn}(\theta, \phi) = r\nabla \mathrm{Y}_{mn}(\theta, \phi) = \left[\frac{\mathrm{d}\,\mathrm{P}_n^m(\cos\theta)}{\mathrm{d}\theta}\hat{\theta} + \mathrm{i}m \frac{\mathrm{P}_n^m(\cos\theta)}{\sin\theta}\hat{\phi}\right] \mathrm{e}^{\mathrm{i}m\phi}. \tag{11}$$

If equations (8) and (9) are multiplied (dot product) by the VSHs $\boldsymbol{m}_{-mn'}(\theta,\phi)$ and $\boldsymbol{n}_{-mn'}(\theta,\phi)$, and then are integrated over the sphere surface (the projection method), we can obtain

$$b_{mn}\xi_n(k_0r_0)-c_{mn}\xi_n^+(k_+r_0)+d_{mn}\xi_n^-(k_-r_0)=\frac{1}{2\pi E_0\Gamma_{mn}}U_{mn}^{\mathrm{e}}, \tag{12}$$

$$a_{mn}h_n^{(1)}(k_0r_0)-c_{mn}j_n(k_+r_0)-d_{mn}j_n(k_-r_0)=\frac{-1}{2\pi E_0\Gamma_{mn}}V_{mn}^{\mathrm{e}}, \tag{13}$$

$$a_{mn}\xi_n(k_0r_0)-c_{mn}\frac{\eta_0}{\eta}\xi_n^+(k_+r_0)-d_{mn}\frac{\eta_0}{\eta}\xi_n^-(k_-r_0)=\frac{\mathrm{i}}{2\pi E_0\Gamma_{mn}}U_{mn}^{\mathrm{h}}, \tag{14}$$

$$b_{mn}h_n^{(1)}(k_0r_0)-c_{mn}\frac{\eta_0}{\eta}j_n(k_+r_0)+d_{mn}\frac{\eta_0}{\eta}j_n(k_-r_0)=\frac{-\mathrm{i}}{2\pi E_0\Gamma_{mn}}V_{mn}^{\mathrm{h}}, \tag{15}$$

where $\Gamma_{mn}=(-1)^m2n(n+1)/(2n+1)$, and

$$\xi_n(k_0r_0)=\frac{1}{k_0r_0}\frac{\mathrm{d}}{\mathrm{d}(k_0r_0)}[k_0r_0h_n^{(1)}(k_0r_0)], \tag{16}$$

$$\xi_n^{\pm}(k_\pm r_0)=\frac{1}{k_\pm r_0}\frac{\mathrm{d}}{\mathrm{d}(k_\pm r_0)}[k_\pm r_0j_n(k_\pm r_0)], \tag{17}$$

$$U_{mn}^{\mathrm{e}}=\int_0^{\pi}\int_0^{2\pi}\boldsymbol{E}^{\mathrm{i}}\big|_{r=r_0}\times\boldsymbol{m}_{-mn}\cdot\hat{r}\sin\theta\,\mathrm{d}\theta\,\mathrm{d}\phi, \tag{18}$$

$$V_{mn}^{\mathrm{e}}=\int_0^{\pi}\int_0^{2\pi}\boldsymbol{E}^{\mathrm{i}}\big|_{r=r_0}\times\boldsymbol{n}_{-mn}\cdot\hat{r}\sin\theta\,\mathrm{d}\theta\,\mathrm{d}\phi, \tag{19}$$

$$U_{mn}^{\mathrm{h}}=\int_0^{\pi}\int_0^{2\pi}\eta_0\boldsymbol{H}^{\mathrm{i}}\big|_{r=r_0}\times\boldsymbol{m}_{-mn}\cdot\hat{r}\sin\theta\,\mathrm{d}\theta\,\mathrm{d}\phi, \tag{20}$$

$$V_{mn}^{\mathrm{h}}=\int_0^{\pi}\int_0^{2\pi}\eta_0\boldsymbol{H}^{\mathrm{i}}\big|_{r=r_0}\times\boldsymbol{n}_{-mn}\cdot\hat{r}\sin\theta\,\mathrm{d}\theta\,\mathrm{d}\phi. \tag{21}$$

In deriving Eqs. (12)–(15), the following formula are used:

$$\int_0^{\pi}\left[\frac{\mathrm{d}\,\mathrm{P}_n^{-m}(\cos\theta)}{\mathrm{d}\theta}\frac{\mathrm{d}\,\mathrm{P}_n'^{m}(\cos\theta)}{\mathrm{d}\theta}+m^2\frac{\mathrm{P}_n^{-m}(\cos\theta)}{\sin\theta}\frac{\mathrm{P}_n'^{m}(\cos\theta)}{\sin\theta}\right]\sin\theta\,\mathrm{d}\theta=\begin{cases}0, & n'\neq n,\\ \Gamma_{mn}, & n'=n,\end{cases} \tag{22}$$

$$\int_0^{\pi}m\left[\frac{\mathrm{d}\,\mathrm{P}_n^{-m}(\cos\theta)}{\mathrm{d}\theta}\frac{\mathrm{P}_n'^{m}(\cos\theta)}{\sin\theta}+\frac{\mathrm{P}_n^{-m}(\cos\theta)}{\sin\theta}\frac{\mathrm{d}\,\mathrm{P}_n'^{m}(\cos\theta)}{\mathrm{d}\theta}\right]\sin\theta\,\mathrm{d}\theta=0. \tag{23}$$

The validity of theoretical procedures above can be easily proved. The incident EM fields are expanded, as usual, in terms of the SVWFs of the first kind as follows:

$$\boldsymbol{E}^{\mathrm{i}}=E_0\sum_{n=1}^{\infty}\sum_{m=-n}^{n}[G_{n,\mathrm{TE}}^m\boldsymbol{M}_{mn}^{r(1)}(k_0\boldsymbol{r})+G_{n,\mathrm{TM}}^m\boldsymbol{N}_{mn}^{r(1)}(k_0\boldsymbol{r})], \tag{24}$$

$$\boldsymbol{H}^{\mathrm{i}}=-\mathrm{i}E_0\frac{1}{\eta_0}\sum_{n=1}^{\infty}\sum_{m=-n}^{n}[G_{n,\mathrm{TE}}^m\boldsymbol{N}_{mn}^{r(1)}(k_0\boldsymbol{r})+G_{n,\mathrm{TM}}^m\boldsymbol{M}_{mn}^{r(1)}(k_0\boldsymbol{r})], \tag{25}$$

By substituting Eqs. (24) and (25) into Eqs. (12)–(15) and then considering Eqs. (22) and (23), the relationship can be readily obtained among the expansion coefficients of the incident laser beam, internal and scattered fields, which is equivalent to the exact analytical solution following the generalized Lorenz–Mie theory (GLMT),[6,10,11], *i.e.*, Eqs. (20)–(23) in Ref. [6].

The integrations over the sphere surface in Eqs. (18)–(21) are numerically evaluated, *e.g.*, by Simpson's 13 rule in our programming with MATLAB, for which the integration expressions are provided for two examples as shown below.

$$U_{mn}^{\mathrm{e}}=-\int_0^{\pi}\int_0^{2\pi}\left(E_\theta^{\mathrm{i}}\frac{\mathrm{d}\,\mathrm{P}_n^{-m}(\cos\theta)}{\mathrm{d}\theta}+E_\phi^{\mathrm{i}}\,\mathrm{i}(-m)\frac{\mathrm{P}_n^{-m}(\cos\theta)}{\sin\theta}\right)\mathrm{e}^{-\mathrm{i}m\phi}\sin\theta\,\mathrm{d}\theta\,\mathrm{d}\phi, \tag{26}$$

$$V_{mn}^{\mathrm{e}}=\int_0^{\pi}\int_0^{2\pi}\left(E_\theta^{\mathrm{i}}\,\mathrm{i}(-m)\frac{\mathrm{P}_n^{-m}(\cos\theta)}{\sin\theta}-E_\phi^{\mathrm{i}}\frac{\mathrm{d}\,\mathrm{P}_n^{-m}(\cos\theta)}{\mathrm{d}\theta}\right)\mathrm{e}^{-\mathrm{i}m\phi}\sin\theta\,\mathrm{d}\theta\,\mathrm{d}\phi, \tag{27}$$

where E_θ^{i} and E_ϕ^{i} are respectively the θ and ϕ component of $\boldsymbol{E}^{\mathrm{i}}$.

From Eqs. (12)–(15), the expansion coefficients can be determined as follows:

$$\begin{pmatrix}a_{mn} & b_{mn} & c_{mn} & d_{mn}\end{pmatrix}=\frac{1}{T_n}\begin{pmatrix}T_{mn}^a & T_{mn}^b & T_{mn}^c & T_{mn}^d\end{pmatrix}, \tag{28}$$

where

$$\begin{aligned}T_n=&\,\mathrm{h}_n^{(1)}(k_0r_0)\xi_n(k_0r_0)\left[1+\left(\frac{\eta_0}{\eta}\right)^2\right]E_n\\&-2\frac{\eta_0}{\eta}\left\{\left[\mathrm{h}_n^{(1)}(k_0r_0)\right]^2\xi_n^+(k_+r_0)\xi_n^-(k_-r_0)+\xi_n^2(k_0r_0)j_n(k_+r_0)j_n(k_-r_0)\right\},\end{aligned} \tag{29}$$

$$T_{mn}^{\mathrm{a}}=\frac{1}{2\pi E_0\Gamma_{mn}}\Big\{\left[U_{mn}^{\mathrm{e}}\mathrm{h}_n^{(1)}(k_0r_0)+\mathrm{i}V_{mn}^{h}\xi_n(k_0r_0)\right]\frac{\eta_0}{\eta}F_n+\left[\mathrm{i}U_{mn}^{\mathrm{h}}\mathrm{h}_n^{(1)}(k_0r_0)-V_{mn}^{\mathrm{e}}\left(\frac{\eta_0}{\eta}\right)^2\xi_n(k_0r_0)\right]E_n$$
$$+2\frac{\eta_0}{\eta}\left[V_{mn}^{\mathrm{e}}\mathrm{h}_n^{(1)}(k_0r_0)\xi_n^{+}(k_+r_0)\xi_n^{-}(k_-r_0)-\mathrm{i}U_{mn}^{h}\xi_n(k_0r_0)j_n(k_+r_0)j_n(k_-r_0)\right]\Big\},\tag{30}$$

$$T_{mn}^{\mathrm{b}}=\frac{1}{2\pi E_0\Gamma_{mn}}\Big\{\left[V_{mn}^{\mathrm{e}}\xi_n(k_+r_0)+\mathrm{i}U_{mn}^{\mathrm{h}}\mathrm{h}_n^{(1)}(k_0r_0)\right]\frac{\eta_0}{\eta}F_n+\left[U_{mn}^{\mathrm{e}}\mathrm{h}_n^{(1)}(k_0r_0)\left(\frac{\eta_0}{\eta}\right)^2-\mathrm{i}V_{mn}^{\mathrm{h}}\xi_n(k_0r_0)\right]E_n$$
$$+2\frac{\eta_0}{\eta}\left[\mathrm{i}V_{mn}^{\mathrm{h}}\mathrm{h}_n^{(1)}(k_0r_0)\xi_n^{+}(k_+r_0)\xi_n^{-}(k_-r_0)-U_{mn}^{\mathrm{e}}\xi_n(k_0r_0)j_n(k_+r_0)j_n(k_-r_0)\right]\Big\},\tag{31}$$

$$T_{mn}^{\mathrm{c}}=\frac{1}{2\pi E_0\Gamma_{mn}}\Big\{\left[U_{mn}^{\mathrm{e}}\mathrm{h}_n^{(1)}(k_0r_0)+\mathrm{i}V_{mn}^{\mathrm{h}}\xi_n(k_0r_0)\right]\times\left[\mathrm{h}_n^{(1)}(k_0r_0)\frac{\eta_0}{\eta}\xi_n^{-}(k_-r_0)-\xi_n(k_0r_0)j_n(k_-r_0)\right]$$
$$+\left[V_{mn}^{\mathrm{e}}\xi_n(k_0r_0)+\mathrm{i}U_{mn}^{\mathrm{h}}\mathrm{h}_n^{(1)}(k_0r_0)\right]\left[\mathrm{h}_n^{(1)}(k_0r_0)\xi_n^{-}(k_-r_0)-\xi_n(k_0r_0)\frac{\eta_0}{\eta}j_n(k_-r_0)\right]\Big\},\tag{32}$$

$$T_{mn}^{\mathrm{d}}=\frac{1}{2\pi E_0\Gamma_{mn}}\Big\{\left[U_{mn}^{\mathrm{e}}\mathrm{h}_n^{(1)}(k_0r_0)+\mathrm{i}V_{mn}^{\mathrm{h}}\xi_n(k_0r_0)\right]\times\left[\xi_n(k_0r_0)j_n(k_+r_0)-\mathrm{h}_n^{(1)}(k_0r_0)\frac{\eta_0}{\eta}\xi_n^{+}(k_+r_0)\right]$$
$$+\left[V_{mn}^{\mathrm{e}}\xi_n(k_0r_0)+\mathrm{i}U_{mn}^{\mathrm{h}}\mathrm{h}_n^{(1)}(k_0r_0)\right]\left[\mathrm{h}_n^{(1)}(k_0r_0)\xi_n^{+}(k_+r_0)-\xi_n(k_0r_0)\frac{\eta_0}{\eta}j_n(k_+r_0)\right]\Big\},\tag{33}$$

$$E_n=j_n(k_+r_0)\xi_n^{-}(k_-r_0)+j_n(k_-r_0)\xi_n^{+}(k_+r_0),\tag{34}$$

$$F_n=j_n(k_+r_0)\xi_n^{-}(k_-r_0)-j_n(k_-r_0)\xi_n^{+}(k_+r_0).\tag{35}$$

By substituting a_{mn} and b_{mn} into Eqs. (1) and (2), and c_{mn} and d_{mn} into Eqs. (5) and (6), the scattered field and the internal fields can be obtained.

3. Numerical results

In this paper, the normalized internal and near-surface FID are calculated, which are defined by

$$|\boldsymbol{E}^{\mathrm{w}}/E_0|^2=(|E_r^{\mathrm{w}}|)^2+|E_\theta^{\mathrm{w}}|^2+\left|E_\phi^{\mathrm{w}}\right|^2/|E_0|^2\tag{36}$$

and

$$\left|\frac{(\boldsymbol{E}^{\mathrm{i}}+\boldsymbol{E}^{\mathrm{s}})}{E_0}\right|^2=\frac{\left(\left|E_r^{\mathrm{i}}+E_r^{\mathrm{s}}\right|^2+\left|E_\theta^{\mathrm{i}}+E_\theta^{\mathrm{s}}\right|^2+\left|E_\phi^{\mathrm{i}}+E_\phi^{\mathrm{s}}\right|^2\right)}{|E_0|^2},\tag{37}$$

where the subscripts r, θ, and ϕ denote the r, θ, and ϕ components of the electric fields, respectively.

When studying the scattering of laser beams by spherical objects,[6–8] the usual analytical method needs to expand the incident beams with SVWFs. As common laser beams, such as Gaussian beam, Hermite–Gaussian beam, Laguerre–Gaussian beam or Bessel beam, can be only described approximately to a higher degree to satisfy Maxwell equations, which makes them very difficult expanded with SVWFs. According to previous researches, in this paper we present the projection method, *i.e.*, multiplying both sides of the EM boundary conditions by VSHs and integrating them on the spherical surface. It is only necessary to know the expression of the beam description, rather than to obtain the SVWF expansion of the beam. The results obtained by the projection method are in agreement with those obtained by the analytical method, which have been verified by the theoretical and numerical results of Gaussian beams with known SVWF expansions. The scattering of common beams (Gaussian beam, Hermite–Gaussian beam, Laguerre–Gaussian beam, and Bessel beam) by chiral spherical objects is calculated. Unlike the scattered far-field reported in most of published papers, the near-field and internal-field characteristics of the chiral sphere irradiated by EM beam are studied in detail in this paper. These properties are very important for studying the properties of chiral media, and also for manipulating the optical tweezers and imaging the particles with super-resolution.

For the incidence of a fundamental Gaussian beam ($\mathrm{TEM}_{00}^{(x')}$ mode focused laser beam) described by the Davis–Barton third-order corrected expressions (see Appendix A),[12–14] the normalized internal and near-surface FIDs for a chiral sphere are shown in Fig. 2. Numerical results show that the incident Gaussian beam is focused within the chiral sphere when propagating. Comparing with Fig. 2(b), the chiral sphere in Fig. 2(c) deviates from the Gaussian beam center. Although the focal position is unchanged within the chiral sphere, the normalized FIDs become asymmetrical and the maximum intensity is reduced by about 70%, which is suitable for the stable capture of particles in the optical tweezer system.

As discussed in Ref. [14], expressions of EM components for a higher-order Hermite–Gaussian beam can be derived by taking transverse derivatives of $\mathrm{TEM}_{00}^{(x',y')}$ as

$$\mathrm{TEM}_{mn}^{(x',y')}=\frac{\partial^m\partial^n\mathrm{TEM}_{00}^{(x',y')}}{\partial\xi^m\partial\eta^n}.$$

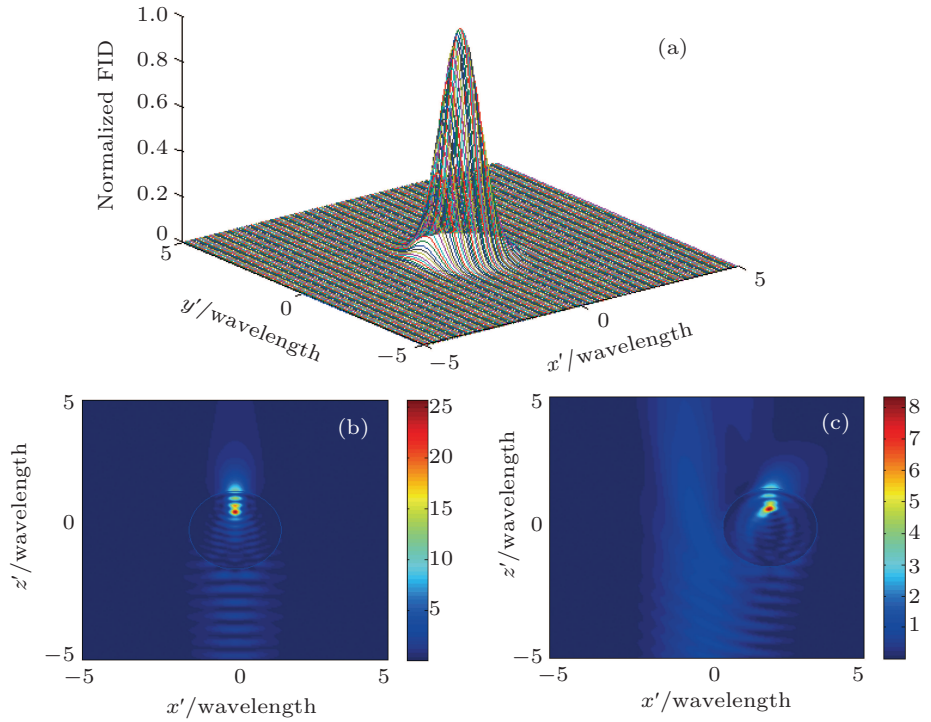


Fig. 2. (a) Normalized FID for $\mathrm{TEM}_{00}^{(x')}$ mode focused laser beam ($w_0 = 2\lambda$) in $x'O'y'$ plane. Normalized FIDs in $x'O'z'$ plane for chiral sphere ($k_0 r_0 = 3\pi$, $\varepsilon_r = 4$, $\mu_r = 1$, $\kappa = 0.5$) illuminated by the above focused laser beam respectively with (b) ($x'_0 = y'_0 = z'_0 = 0$) and (c) ($x'_0 = 2\lambda$, $y'_0 = z'_0 = 0$).

Figure 3 shows the normalized internal and near-surface FID for a chiral sphere under the illumination of a $\mathrm{TEM}_{10}^{(x)}$ mode Hermite–Gaussian beam. It is demonstrated in Fig. 3(c) that the FID profile is symmetrical about origin O', while for the case of a dielectric sphere the FID profile is symmetrical about the axis $O'y'$.[13]

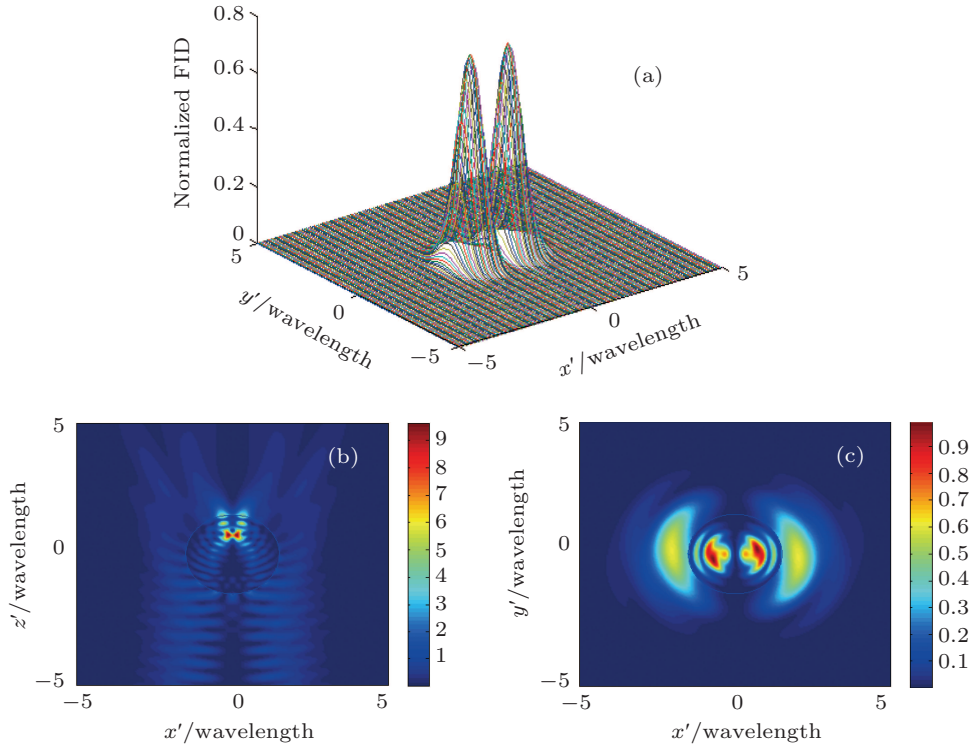


Fig. 3. (a) Normalized FID for $\mathrm{TEM}_{10}^{(x)}$ mode Hermite–Gaussian beam ($w_0 = 2\lambda$) in the $x'O'y'$ plane. Normalized FIDs (b) in the $x'O'z'$ plane and (c) in the $x'O'y'$ plane for the same model as in Fig. 2 ($k_0 r_0 = 3\pi$, $\varepsilon_r = 4$, $\mu_r = 1$, $\kappa = 0.5$), illuminated by the above Hermite–Gaussian beam ($x'_0 = y'_0 = z'_0 = 0$).

Any Laguerre–Gaussian beam can be expressed in a sum of Hermite–Gaussian beams,[14] in which various doughnut mode beams are of particular interest. Figure 4 shows the normalized internal and near-surface FID for a chiral sphere illuminated by a

radial doughnut mode beam created by $\mathrm{TEM}_{dn}^{(\mathrm{rad})} = (\mathrm{TEM}_{10}^{(x')} + \mathrm{TEM}_{01}^{(y')})/\sqrt{2}$. Comparing with the normalized FID in Fig. 4(a) for the doughnut mode beam, in Fig. 4(c) periodical max and min field distributions along the radius direction arise in the FID.

Figures 2(a)–4(a) display the intensity distributions for different types of beams. For each case, the beams described by Figs. 2(a)–4(a) have the same total power, and the beam waist is assumed to be $w_0 = 2\lambda$. Figure 2(a) shows that the maximum intensity occurs at the point ($x' = y' = 0$), and Fig. 3(a) at the point ($x' = \pm 0.707$, $y' = 0$) and Fig. 4(a) at a radius of $r' = 0.707$ from origin O'.

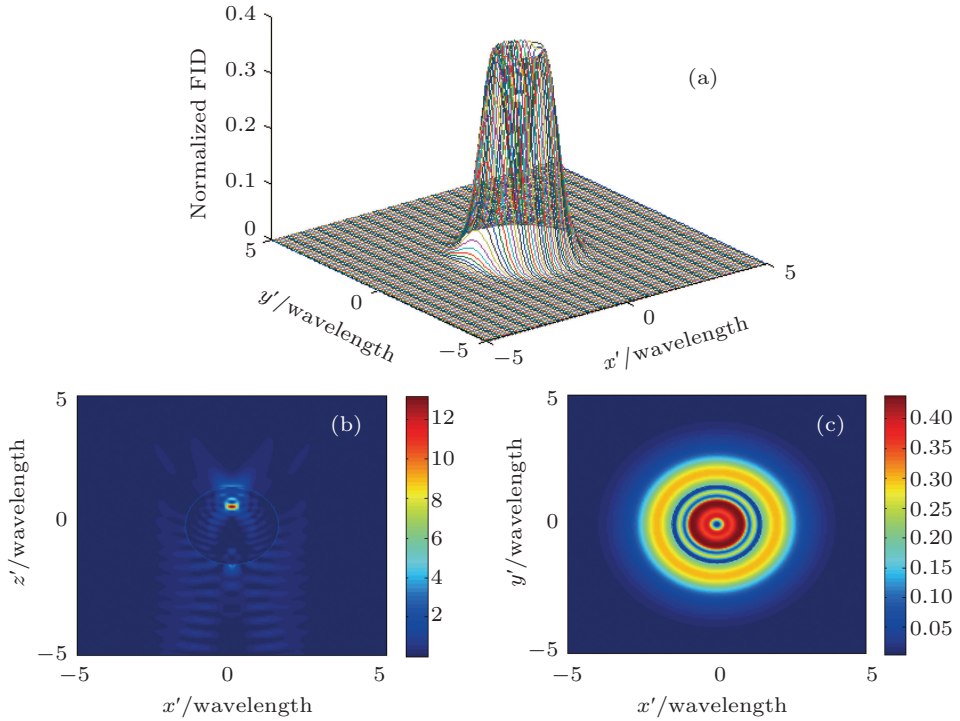


Fig. 4. (a) Normalized FID for $\mathrm{TEM}_{dn}^{(\mathrm{rad})}$ doughnut mode beam ($w_0 = 2\lambda$) in $x'O'y'$ plane. Normalized FID (b) in the $x'O'z'$ plane and (c) in the $x'O'y'$ plane for the same model as in Fig. 2 ($k_0 r_0 = 3\pi$, $\varepsilon_r = 4$, $\mu_r = 1$, $\kappa = 0.5$), illuminated by the above doughnut mode beam ($x'_0 = y'_0 = z'_0 = 0$).

The EM field components of a ZOBB propagating along the positive z' axis in $O'x'y'z'$ have been given in Refs. [15] and [16]. Figure 5 shows the normalized internal and near-surface FID in the $x'O'z'$ plane for a chiral sphere illuminated by a ZOBB with a half-cone angle ψ. From Fig. 5 we can see that the focal region outside the chiral sphere is far from the chiral sphere, and more focal regions appear as well. Thus, the gradient distribution of field intensity is more evident, which is beneficial to cancelling the scattering force and realizing particle capture.

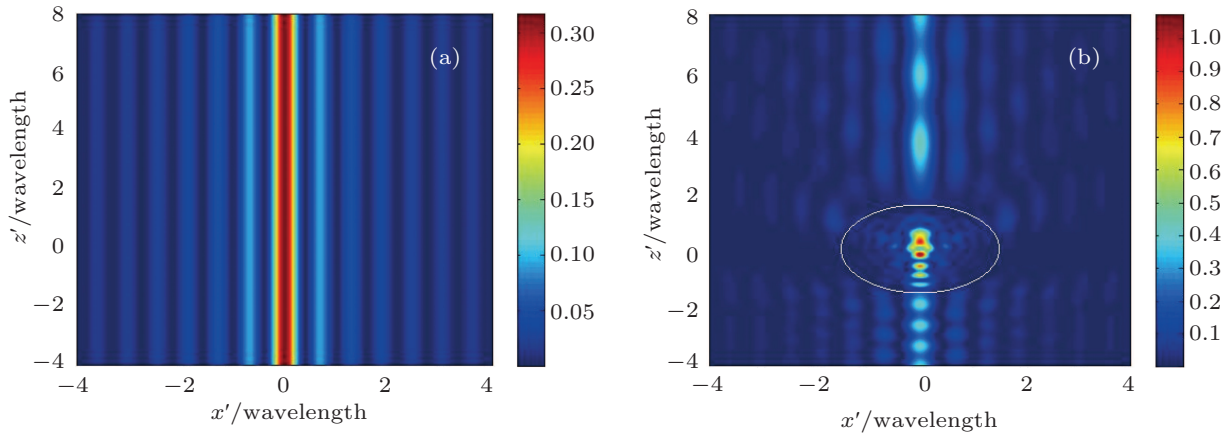


Fig. 5. (a) Normalized FID in $x'O'z'$ plane for ZOBB. (b) Normalized FID in $x'O'z'$ plane for the same model as in Fig. 2 ($k_0 r_0 = 3\pi$, $\varepsilon_r = 4$, $\mu_r = 1$, $\kappa = 0.5$), for chiral sphere illuminated by ZOBB ($\psi = \pi/3$, $x'_0 = y'_0 = z'_0 = 0$).

In Figs. 3– 5 the chiral sphere is located in the middle of incident EM field. As a result, a symmetrical distribution of the field intensity on both sides of the z' axis is observed. The numerical results based on Fig. 3 show that the focused intensity of Hermite-Gaussian beam decreases and its intensity gradient increases obviously when compared with

the scenarios of Gaussian beam. The symmetrical distribution of the light field on both sides of the central axis is beneficial to the formation of a balanced light field. Numerical results based on Fig. 4 show that the intensity of focused beam is between the intensity of Hermite–Gaussian beam and the intensity of Gaussian beam, and the gradient distribution of intensity is stronger than that of Gaussian beam and weaker than that of Hermite–Gaussian beam. Numerical results based on Fig. 5 show that compared with the fundamental Gaussian laser beam, Hermite–Gaussian beam and doughnut mode beam, the ZOBB beam has a focal region that is located in the center of chiral sphere, and the intensity of the light field decreases. For a ZOBB, the gradient distribution of the intensity is more obvious, and the resultant gradient force potential trap enables us to capture the particle conveniently.

4. Conclusions

According to the field expansions in terms of the SVWFs, EM boundary conditions and projection method, a general approach to the accurate calculation of scattering from a chiral sphere is presented and verified. The normalized FIDs of internal and near-surface field are calculated for a variety of structured beams, *e.g.*, the fundamental Gaussian beam, Hermite–Gaussian beam, doughnut mode beam and ZOBB. The focusing position and intensity distribution due to the illumination of different light field are analyzed. This work provides a general solution to arbitrarily structured laser beam scattering from a chiral sphere, and is of significance in relevant fields of atmospheric detection, biotechnology, chemical technology, laser optical tweezers, laser radar detection, *etc*.

Appendix A

Third-order corrected expressions for the EM field components of a fundamental Gaussian laser beam ($\mathrm{TEM}_{00}^{(x')}$ mode focused beam) in $O'x'y'z'$, developed by Barton and Alexander,[12–14] are written as

$$E'_x = E_0[1+s^2(\mathrm{i}Q^3\rho^4 - Q^2\rho^2 - 2Q^2\xi^2)]\psi_0\,\mathrm{e}^{\mathrm{i}\zeta/s^2}, \quad \text{(A1)}$$

$$E'_y = -E_0 s^2 2Q^2\xi\eta\psi_0\,\mathrm{e}^{\mathrm{i}\zeta/s^2}, \quad \text{(A2)}$$

$$E'_z = E_0[s2Q\xi + s^3(2\mathrm{i}Q^4\rho^4\xi - 6Q^3\rho^2\xi)]\psi_0\,\mathrm{e}^{\mathrm{i}\zeta/s^2}, \quad \text{(A3)}$$

$$H'_x = -\frac{E_0}{\eta_0}H_0 s^2 2Q^2\xi\eta\psi_0\,\mathrm{e}^{\mathrm{i}\zeta/s^2}, \quad \text{(A4)}$$

$$H'_y = \frac{E_0}{\eta_0}[1+s^2(\mathrm{i}Q^3\rho^4 - Q^2\rho^2 - 2Q^2\eta^2)]\psi_0\,\mathrm{e}^{\mathrm{i}\zeta/s^2}, \quad \text{(A5)}$$

$$H'_z = \frac{E_0}{\eta_0}[s2Q\eta + s^3(2\mathrm{i}Q^4\rho^4\eta - 6Q^3\rho^2\eta)]\psi_0\,\mathrm{e}^{\mathrm{i}\zeta/s^2}, \quad \text{(A6)}$$

where $\xi = x'/w_0$, $\eta = y'/w_0$, $\zeta = z'/(kw_0^2)$, $\rho^2 = \xi^2+\eta^2$, $Q = 1/(\mathrm{i}-2\zeta)$, $s = 1/(kw_0)$, and $\psi_0(\xi,\eta,\zeta) = \mathrm{i}Q\exp(-\mathrm{i}\rho^2 Q)$ are the non-dimensional parameters, and w_0 is the beam waist radius.

By considering the duality principle, *i.e.*, replacing $\boldsymbol{E}$ in Eqs. (A1)–(A6) by $-\boldsymbol{H}$, $\boldsymbol{H}$ by $\boldsymbol{E}$, ε_0 by μ_0, and μ_0 by ε_0, third-order corrected expressions for a $\mathrm{TEM}_{00}^{(y')}$ mode focused Gaussian beam can be conveniently obtained.

References

[1] Bohren C F 1974 *Chem. Phys. Lett* **29** 458
[2] Fernandez C I, Zambrana P X and Molina T G 2012 *Phys. Rev. A* **86** 042103
[3] Gustavson T L, Chikkatur A P, Leanhardt A E, Gölitz A, Gupta S, Pritchard D E and Ketterle W 2001 *Phys. Rev. Lett.* **88** 020401
[4] Fahrbach F O, Simon P and Rohrbach A 2010 *Nat. Photon.* **4** 780
[5] Yokota M, He S and Takenaka T 2001 *J. Opt. Soc. Am. A* **18** 1681
[6] Zhu X P, Liao T Q, Zhang H Y and Hui R Q 2012 *JQSRT* **113** 1946
[7] Shang Q C, Wu Z S, Qu T, Li Z J and Bai L 2013 *Opt. Express* **21** 8677
[8] Qu T, Wu Z S, Shang Q C and Li Z J 2016 *J. Opt. Soc. Am. A* **33** 475
[9] Stratton J A 1941 *Electromagnetic Theory* (New York: McGraw-Hill) Chap. VII
[10] Gouesbet G, Maheu B and Gréhan G 1988 *J. Opt. Soc. Am. A* **5** 1427
[11] Gouesbet G 2009 *JQSRT* **110** 1223
[12] Davis L W 1979 *Phys. Rev. A* **19** 1177
[13] Barton J P and Alexander D R 1989 *J. Appl. Phys.* **66** 2800
[14] Barton J P 1997 *Appl. Opt.* **36** 1303
[15] Mishra S R 1991 *Opt. Commun.* **85** 159
[16] Mitri F G 2011 *Opt. Lett.* **36** 766